Chapter 14
Intelligent Load Frequency Control in Presence of Wind Power Generation

Nour EL Yakine Kouba and Mohamed Boudour

Abstract With the advent of large-scale interconnected power systems, many new problems have emerged, which include frequency fluctuations problem. In many parts of the world, installed capacity and energy production levels for electric generation from non-conventional renewable resources such as wind power generation are growing rapidly. However, the fluctuations of these generators affect the system frequency. The purpose of this work is to design an intelligent load frequency control (LFC) strategy based on Fuzzy Logic-PID controller to suppress all the fluctuations of the total power output of the wind generation and maintain the constancy of the system frequency. To show the effectiveness of the proposed control strategy, a two-area multi-sources power system was investigated for the simulation. The observed simulation results of the proposed Fuzzy Logic-PID controller are compared with the results obtained by the classical Ziegler-Nichols method and the meta-heuristic Particle Swarm Optimization (PSO) technique. The transient responses showing the integration impact of the wind farm are depicted and the results are tabulated as a comparative performance in view of peak overshoot and settling time. The results are compared and the ability of the proposed approach to evaluate load frequency control over large wind farm integration is confirmed.

Keywords Load frequency control (LFC) · PID controller · Fuzzy logic control (FLC) · Wind power generation · Wind farm

N. EL. Y. Kouba (✉) · M. Boudour
Laboratory of Electrical and Industrial Systems, Faculty of Electrical Engineering and Computing, University of Sciences and Technology Houari Boumediene, Bab Ezzouar, Algiers, Algeria
e-mail: nkouba@ieee.org; mboudour@ieee.org

N. Derbel, Q. Zhu (eds.), *Modeling, Identification and Control Methods in Renewable Energy Systems*, Green Energy and Technology,
https://doi.org/10.1007/978-981-13-1945-7_14

14.1 Introduction

The endeavor for a more sustainable power generation has led to a fast increase in green power generation from renewable energy sources (RES), such as wind, biomass, hydro and solar power. These sources are of a fluctuating nature; consequently, many new challenges must be introduced in power system stability and control. Amongst them, a wind farm type of power generation is considered the most viable alternative (Kouba et al. 2016c,d). The generation of wind energy is clean, exhaustless and more economic. However, this energy is not stable and cannot ensure the constant power generation because it depends on the wind as a natural source (Bevrani and Daneshmand 2012). In addition, a large wind farm can include hundreds of wind turbines and the output of each one of them depends on wind direction and velocity, which result into frequency oscillations (Eduardo et al. 2011; Kouba et al. 2016a). The control of system frequency is a vital aspect for a secure and stable electrical network with good power quality. Frequency control can be called upon for a variety of conditions ranging from a gradual change in load levels over time to a sudden loss of generation or step increase/decrease in load. A continuous balance between active power generated and active power consumed by the load and losses is required to maintain frequency constant at nominal system frequency value within an acceptable tolerance (Patnaik and Dash 2015; Sahu et al. 2013). The frequency and load have an inverse relationship; therefore any imbalance in active power will result in a frequency deviation. Maintaining the frequency at its nominal value requires that both active power produced and consumed be controlled to keep the load and supply in equilibrium. The increasing size of the interconnected power systems has been accompanied with the appearance of the frequency fluctuations problems, which may results in disconnection actions, loss of several lines, zone isolation and black-out. Therefore, the frequency control on an interconnected electrical network is particularly challenging function and can be considered to be one of the most crucial aspects of ancillary services (Bihui et al. 2011; Kouba et al. 2016b). In large-scale interconnected power system, balancing power production and consumption is usually guaranteed by Automatic Generation control (AGC) scheme adjusting production of some power plants to meet the current demand (Ramakrishna and Bhatti 2008). If there is a power mismatch, system frequency will change as the rotating mass in generators will be either accelerated, thus increasing frequency, if too much electric power is produced, or decelerated, thus decreasing frequency, if the demand is bigger than the production (Kiaee et al. 2013; Prakash and Sinha 2014). In the case of any contingencies such as the change in load, failure of a plant or the outage of a line, if no action is taken and the power mismatch remains, system frequency will diverge until a critical point is reached resulting in a black-out, which is an undesirable case. Generally, in the Transmission System Operators (TSOs) the AGC scheme is mapped to three control levels which are: primary, secondary and tertiary control. The primary control is implemented through the governor control system and is used to stabilize the system frequency. The secondary control named also load

frequency control (LFC), reacts slower than primary control and is used to relieve the primary control and restore the system frequency to its pre-disturbance nominal value. Finally, Tertiary control refers to the economic dispatching control (EDC) of each unit and is used to relieve the secondary control loop (LFC) (Kouba et al. 2014b; Tofighi et al. 2015). As major functions of automatic generation control (AGC), power system frequency regulation named load frequency control (LFC) become one of the most important research topics in power system operation. The main goals of LFC are to suppress the fluctuations of the system frequency and maintain the frequency and the power interchanges with neighboring control areas at the scheduled values. To satisfy these objectives, a control error signal called the Area Control Error (ACE) is measured, which represents the real power imbalance between generation and load, where this signal combines both frequency and net interchange flow deviations (Kiaee et al. 2013; Ramakrishna and Bhatti 2008). A PID controller is used to support the frequency regulation LFC loop in each control area, while the measured ACE signal is the input of the PID controller in each control area (Kouba et al. 2014b). In fact, small variations in system frequency will not result in a reduction of system reliability and security. In contrast, large frequency fluctuations in particularly with the increasing integration of renewable energy sources such as wind power generation can have a serious impact on power system equipments and power quality (Chung et al. 2011; Hooshmand et al. 2012). The large increase integration of wind farm in the grid causes extensive changes in power systems, and the generation does not equal scheduled generation at all times, while this mismatch adds to the usual imbalances between supply and demand. However, if a large amount of wind power generation is installed in the grid; it becomes difficult to remove frequency fluctuations. Therefore, it's necessary to study the effects on the frequency control and assess the impact of wind integration. In the aim to balance the deviation between power production and power demand in presence of a large penetration of wind power generation, a robust LFC controller scheme is needed to satisfy these objectives. Various studies consider new control methods dealing with the design of the secondary frequency controller (LFC) have been proposed and discussed in last decades. In 1942, Ziegler and Nichols proposed two heuristic approaches based on their experience and some simulations to quickly adjust the controller parameters: P, PI, and PID (Kouba et al. 2014b). Many others techniques were used for tuning the PID controller parameters such as the stochastic particle swarm optimization (PSO) (RamaSudha et al. 2010), bacterial foraging optimization algorithm (BFOA) (Nanda et al. 2009), hybrid algorithm between bacterial foraging and particle swarm optimization (BF-PSO) (Kouba et al. 2014a), genetic algorithm (GA) (Demirören et al. 2002; Panda and Yegireddy 2013), differential evolution algorithm (DEA) (Pandey et al. 2013), firefly algorithm (FA) (Saikia and Sahu 2013), and many others strategies have been proposed for the LFC study such as the artificial neural network (ANN) (Kouba et al. 2014c; Mahabuba and Khan 2009; Saikia et al. 2011) and H-infinity techniques (Singh et al. 2013). In this work, a dynamic study of the load frequency control (LFC) with a large penetration of wind power generation is presented. The LFC problem has been analyzed using a new algorithm based on the implicit integration

Trapezoidal rule with variable time step and iterative Newton-Raphson method. The wind farm is modeled using a high-number of wind turbines and its impact on the system frequency and the tie-line power flow is examined. A dynamic model of the IEE Japan East 107-bus 30-generator power system is investigated for the purpose of studying long-term frequency stability and control on an interconnected two-area power system concerning high penetration of wind farm. The obtained results are compared to the classical LFC based Ziegler-Nichols method and, thereby to the optimal LFC based particle swarm optimization (PSO) technique. This work is organized as follows. In Sect. 14.2, the interconnected power system model is presented. In Sect. 14.3, the Load Frequency Control (LFC) model is described, and the algorithm used for the frequency stability analysis in this work is explained in detail. Section 14.4 illustrates the proposed Fuzzy Logic-PID controller technique. Section 14.5 is devoted to the modeling of the wind farm. Results of the wind farm integration analysis are given and discussed in Sect. 14.6. Finally, Sect. 14.7 includes the conclusion of this work.

14.2 Interconnected Power System Model

To investigate the performance of the proposed control strategy, the multi-machines power generation (hydro, thermal, and nuclear) IEE Japan East is considered as the test system. This electrical system is widely used in the literature as a standard system for testing of new power system analysis and control strategies. Figure 14.1 shows a single-line diagram of the test system (Arita et al. 2006). This electrical network consists of 107 buses, 30 generators, 31 loads, 191 branches, 136 transmission lines and 55 transformers. The power system is divided to two interconnected control areas. All power generating units in the power system are equipped with generator, turbine and speed governor. The interconnection between the control areas is made using a tie-line power flow. It is noted that, outputs of hydro, thermal and nuclear power plants are controlled automatically with the LFC signal.

In this work, all proposed thermal and nuclear units are modeled with an equivalent thermal unit and all proposed hydro power plans are modeled with an equivalent hydro unit. For the load frequency control study, a classical model of synchronous machine is needed, which includes the mechanicals equations of the generator (swing equation) and the speed regulation system (governor-turbine) model. In our problem, the differential equations representing dynamics of rotating machines are linearized by a numerical integration method, such as the implicit integration Trapezoidal rule, and solved using the iterative Newton-Raphson method for each time step Δt. The control loop model of a synchronous machine which is used in this work is shown in Fig. 14.2.

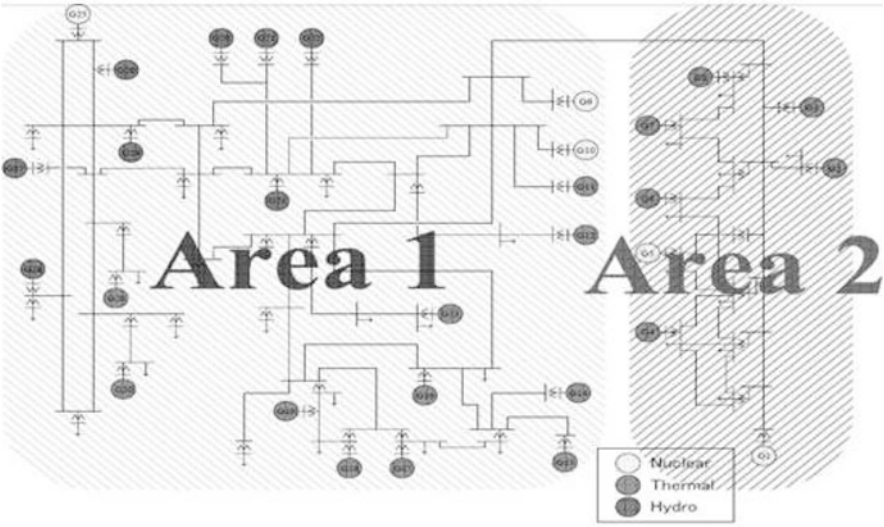

Fig. 14.1 IEE Japan East 107-bus 30-machine power system model

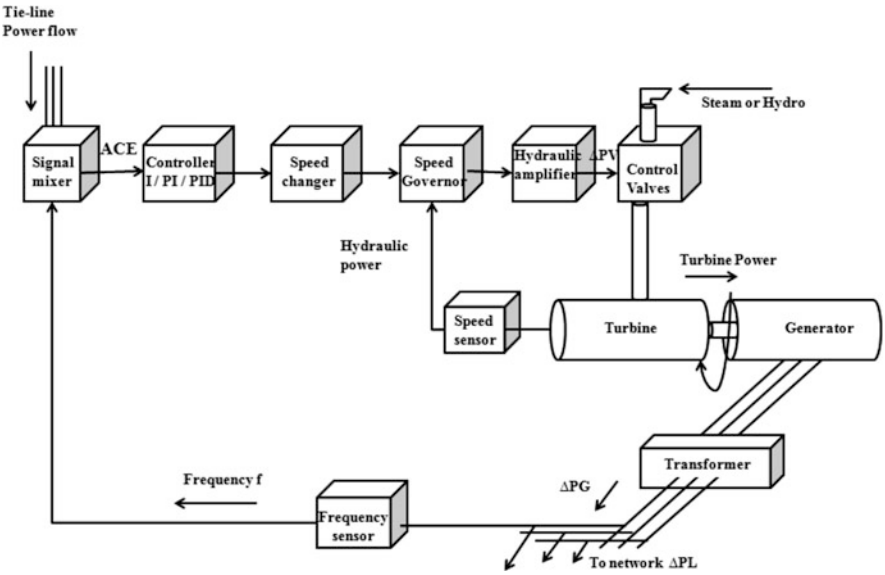

Fig. 14.2 Load frequency control loop of a synchronous machine

14.2.1 Generator Model

The relationship between the mechanical power ΔP_m and the electrical power ΔP_e is given by Arita et al. (2006):

$$M\frac{d\Delta\omega}{dt} = \Delta P_m - \Delta P_e \tag{14.1}$$

The load in a power system is the sum of various power demands and varies randomly over time. Some loads depend on the change of frequency and others don't. In general, the expression of the electrical power which depends on the frequency change can be expressed by Kouba et al. (2014b):

$$\Delta P_e = \Delta P_L + D\Delta\omega \tag{14.2}$$

In multi-machines system, if all generators are assumed to turn with the same speed of synchronism, the equations of the equivalent generator can be expressed with:

- The equivalent inertia constant:

$$M_{eq} = \frac{\sum_{i=1}^{i=n} M_i}{n} \tag{14.3}$$

- The equivalent load-damping constant:

$$D_{eq} = \frac{\sum_{i=1}^{i=n} D_i}{n} \tag{14.4}$$

The block diagram representation of equivalent generator used in this work is shown in Fig. 14.3.

The equivalent generator can be expressed by the following equation:

$$\frac{d\Delta\omega}{dt} = \frac{1}{M_{eq}}\left[\Delta P_{mth} + \Delta P_{mh} - (\alpha\Delta P_{tie}) - \Delta P_L - (D_{eq}\Delta\omega)\right] \tag{14.5}$$

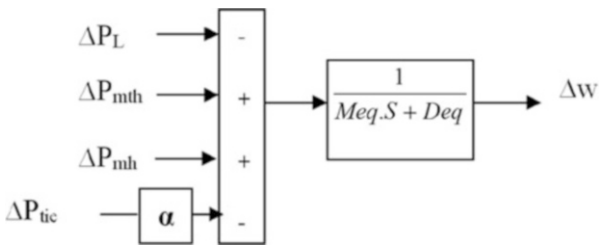

Fig. 14.3 Block diagram representation of equivalent generator

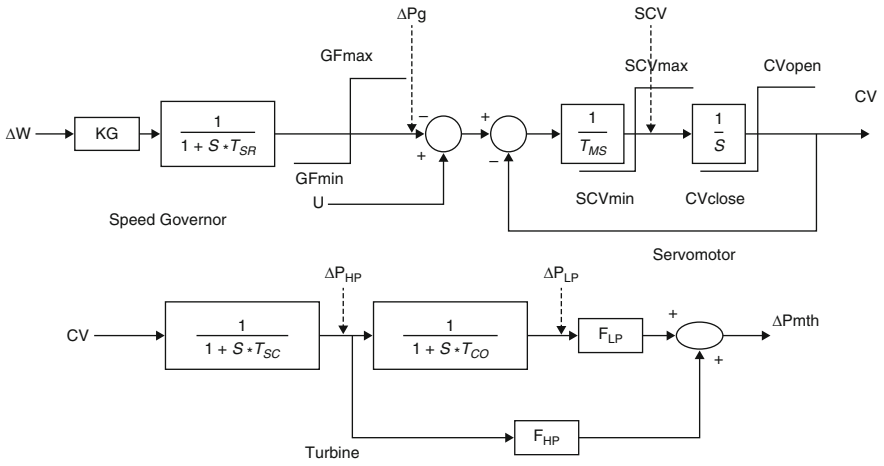

Fig. 14.4 Block diagram of governor-turbine model for thermal/nuclear unit

14.2.2 Governor-Turbine System Model

The main role of a speed governor control system is to adjust the turbine valve to stabilize the system frequency. The schematics of such governors control systems used in this work are shown in Fig. 14.4 for the thermal and nuclear unit and in Fig. 14.5 for the hydro unit (Kouba et al. 2014b).

The equations representing the thermal/nuclear power plant are given by:

$$\begin{cases} \dfrac{d\Delta P_g}{dt} = \dfrac{1}{T_{SR}}(K_G \Delta\omega - \Delta P_g) \\ With: \quad GF_{min} < \Delta P_g < GF_{max} \end{cases} \tag{14.6}$$

$$\begin{cases} SCV = \dfrac{1}{T_{SM}}(U - \Delta P_g - CV) \\ With: \quad SCV_{min} < SCV < SCV_{max} \end{cases} \tag{14.7}$$

$$\begin{cases} \dfrac{dCV}{dt} = \dfrac{1}{T_{SM}}(U - \Delta P_g - CV) \\ With: \quad CV_{close} < CV < CV_{open} \end{cases} \tag{14.8}$$

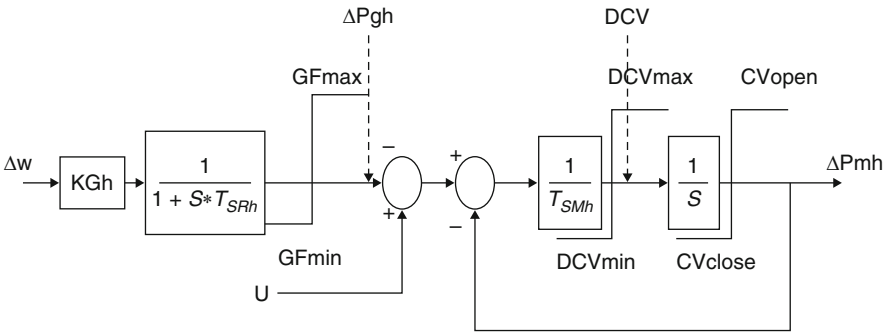

Fig. 14.5 Block diagram of governor-turbine model for hydro unit

$$\begin{cases} \dfrac{d\Delta P_{HP}}{dt} = \dfrac{1}{T_{SC}}(CV - \Delta P_{HP}) \\ \dfrac{d\Delta P_{LP}}{dt} = (\dfrac{1}{T_{CO}})(\Delta P_{HP} - \Delta P_{LP}) \end{cases} \tag{14.9}$$

The mechanical power for the thermal unit is calculated by this expression:

$$\Delta P_{mth} = (F_{HP}\Delta P_{HP}) + (F_{LP}\Delta P_{LP}) \tag{14.10}$$

The equations representing the hydro power plant are given by:

$$\begin{cases} \dfrac{d\Delta P_{gh}}{dt} = (\dfrac{1}{T_{SRH}})((\Delta\omega K_{Gh}) - \Delta P_{gh}) \\ With: \quad GF_{min} < \Delta P_{gh} < GF_{max} \end{cases} \tag{14.11}$$

$$\begin{cases} DCV = (\dfrac{1}{T_{SMh}})(U - \Delta P_{gh} - \Delta P_{mh}) \\ With: \quad DCV_{min} < DCV < DCV_{max} \end{cases} \tag{14.12}$$

$$\begin{cases} \dfrac{d\Delta P_{mh}}{dt} = (\dfrac{1}{T_{SMh}})(U - \Delta P_{gh} - \Delta P_{mh}) \\ With: \quad CV_{close} < CV < CV_{open} \end{cases} \tag{14.13}$$

14.2.3 Tie-Line Model

Using DC load flow method and assuming that the tie-line is from area-1 to area-2, the deviation ΔP_{12} from the nominal flow can be expressed (Kouba et al. 2014a) by:

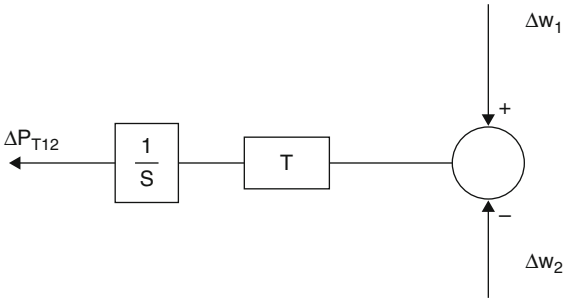

Fig. 14.6 Block diagram of the tie-line power flow model

$$\frac{d\Delta P_{tie}}{dt} = T_{12}(\Delta\omega_1 - \Delta\omega_2) \tag{14.14}$$

The block diagram representation for the tie-line is shown in Fig. 14.6.

14.3 Load Frequency Control (LFC) Model

The frequency has an inverse relationship with the load that is changing continually. Hence, the change in real power affects the system frequency. To maintain the system frequency constant, the power supply must follow the momentary power load change. Corresponding to the demand fluctuation, three control strategies as mentioned in the introduction are used in the electrical network to solve frequency fluctuation problem. The primary control: is a local control through the speed governor control system, is used to stabilize the frequency and is effective for the load change within ten seconds of the disturbance. The secondary control: named the load frequency control (LFC) is used for the disturbance with the period of several minutes to about 30 min. The objective of the LFC loop is to adjust operating point reference of governor in the control area and maintain the system frequency at the nominal value. The tertiary control: refers to the economic dispatching control (EDC) of units, and presents a part of the regular market clearing mechanism. Tertiary control acts on minute-to-hours time scale (30 min–h) (Kassem et al. 2013; Liu et al. 2015; Pan and Das 2015; Pandey et al. 2013; Rahmani and Sadati 2013). In large and interconnected power systems, the load frequency control is considered as the most important control strategy to remove the fluctuations with a long-period. In the centralized LFC model, to evaluate the area requirement (AR), the actual frequency and net interchange power flow are measured by the independent system operator (ISO). The LFC output power signal is sent to each generator when the frequency deviation is detected. Then, each speed governor output of the selected power plant is adjusted by the LFC signal to change the power plant output. To better understanding the function of LFC, Fig. 14.7 depicts the general LFC algorithm. To keep the system frequency and power balance at the scheduled values, each generator is equiped with PID controller. The PID parameters are tuned using the

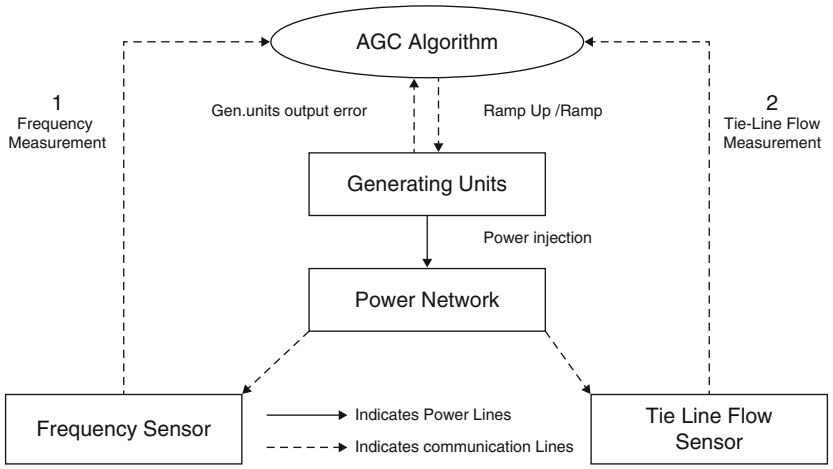

Fig. 14.7 AGC/LFC algorithm

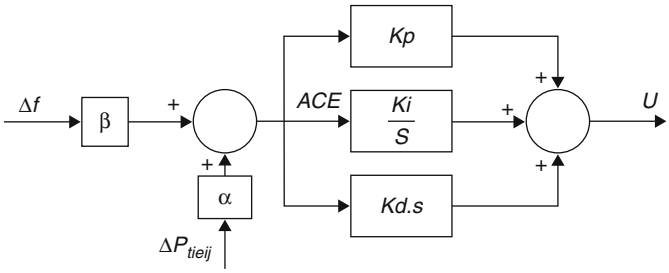

Fig. 14.8 Block diagram of LFC model

traditional Ziegler-Nichols method, the meta-heuristic particle swarm optimization (PSO) algorithm, and the Fuzzy Logic (FL) strategy. The diagram of the LFC model used in this work is shown in Fig. 14.8 (Kouba et al. 2014a). The input signal of each PID controller is the area control error (ACE), which is given by:

$$ACE_i = \alpha \Delta P_{tie} + \beta_{fi} \Delta \omega_i \tag{14.15}$$

The control equation U in each control area is given by:

$$U = ACE\left(K_p + \frac{K_i}{S} + K_d S\right) \tag{14.16}$$

In order to analyze the LFC problem in the two-area interconnected power system, the differential equations system in Eq. (14.17) is algebraized using the implicit Trapezoidal integration rule. After that, the resulting algebraic equations are solved using the iterative Newton-Raphson method at each time step based on

the work developed in Kouba et al. (2014b). By application of implicit integration Trapezoidal rule with a variable integration time step ($h = \Delta t$), the following equations can be obtained:

$$F = \left[X_{n+1} - \frac{\Delta t}{2} f(X_{n+1}, t_{n+1})\right] - \left[X_n + \frac{\Delta t}{2} f(X_n, t_n)\right] \tag{14.17}$$

The differential equations system for the LFC analysis is given by:

$$\begin{cases} \dfrac{d\Delta P_g}{dt} = \dfrac{1}{T_{SR}}(K_G \Delta\omega - \Delta P_g) \\ \dfrac{dCV}{dt} = \dfrac{1}{T_{SM}}(U - \Delta P_g - CV) \\ \dfrac{d\Delta P_{HP}}{dt} = \dfrac{1}{T_{SC}}(CV - \Delta P_{HP}) \\ \dfrac{d\Delta P_{LP}}{dt} = \dfrac{1}{T_{CO}}(\Delta P_{HP} - \Delta P_{LP}) \\ \dfrac{d\Delta P_{gh}}{dt} = \dfrac{1}{T_{SRH}}(K_{Gh}\Delta\omega - \Delta P_{gh}) \\ \dfrac{d\Delta P_{mh}}{dt} = \dfrac{1}{T_{SMh}}(U - \Delta P_{gh} - \Delta P_{mh}) \\ \dfrac{d\Delta\omega}{dt} = \dfrac{1}{M_{eq}}(\Delta P_{mth} + \Delta P_{mh} - \alpha\Delta P_{tie} - \Delta P_L - D_{eq}\Delta\omega) \\ \dfrac{dU_I}{dt} = K_I(\alpha\Delta P_{tie} - \beta_f\Delta\omega) \\ \dfrac{d\Delta P_{tie}}{dt} = T_{12}(\Delta\omega_1 - \Delta\omega_2) \end{cases} \tag{14.18}$$

By applying Eq. (14.17) to the deferential equations system (14.18), the obtained algebraic equations system is given in (14.20), where:

$$F_{1(j,i)} = \begin{bmatrix} F_{11(j,i)} \\ F_{12(j,i)} \\ F_{13(j,i)} \\ F_{14(j,i)} \end{bmatrix};\ F_{2(j,i)} = \begin{bmatrix} F_{21(j,i)} \\ F_{22(j,i)} \end{bmatrix};\ F_{3(i)} = \begin{bmatrix} F_{31(i)} \\ F_{32(i)} \end{bmatrix};\ F_{4(i)} = \begin{bmatrix} F_{4(i)} \end{bmatrix}$$

$$F = [F_1, F_2, F_3, F_4]^t \tag{14.19}$$

At each time step h, the equation $[F] = 0$ is solved by Eq. (14.21).

$$
\begin{cases}
F_{11}(x_n+1,x_n) = \left[\Delta P_{g_{n+1}} - \dfrac{\Delta t}{2T_{SR}}(K_G\Delta\omega_{n+1} - \Delta P_{g_{n+1}})\right] \\
\qquad\qquad - \left[\Delta P_{g_n} + \dfrac{\Delta t}{2T_{SR}}[((\Delta\omega_n K_G) - \Delta P_{g_n})]\right] \\
F_{12}(x_n+1,x_n) = \left[CV_{n+1} - \dfrac{\Delta t}{2T_{SM}}(U_{n+1} - \Delta P_{g_{n+1}} - CV_{n+1})\right] \\
\qquad\qquad - \left[CV_n + \dfrac{\Delta t}{2T_{SM}}(U_n - \Delta P_{g_n} - CV_n)\right] \\
F_{13}(x_n+1,x_n) = \left[\Delta P_{HP_{n+1}} - \dfrac{\Delta t}{2T_{SC}}(CV_{n+1} - \Delta P_{HP_{n+1}})\right] \\
\qquad\qquad - \left[\Delta P_{HP_n} + \dfrac{\Delta t}{2T_{SC}}(CV_n - \Delta P_{HP_n})\right] \\
F_{14}(x_n+1,x_n) = \left[\Delta P_{LP_{n+1}} - \dfrac{\Delta t}{2T_{CO}}(\Delta P_{HP_{n+1}} - \Delta P_{LP_{n+1}})\right] \\
\qquad\qquad - \left[\Delta P_{LP_n} + \dfrac{\Delta t}{2T_{CO}}(\Delta P_{HP_n} - \Delta P_{LP_n})\right] \\
F_{21}(x_n+1,x_n) = \left[\Delta P_{gh_{n+1}} - \dfrac{\Delta t}{2T_{SRH}}(K_{Gh}\Delta\omega_{n+1} - \Delta P_{gh_{n+1}})\right] \\
\qquad\qquad - \left[\Delta P_{gh_n} + \dfrac{\Delta t}{2T_{SRH}}(K_{Gh}\Delta\omega_n - \Delta P_{gh_n})\right] \\
F_{22}(x_n+1,x_n) = \left[\Delta P_{mh_{n+1}} - \dfrac{\Delta t}{2T_{SMh}}(U - \Delta P_{gh_{n+1}} - \Delta P_{mh_{n+1}})\right] \\
\qquad\qquad - \left[\Delta P_{mh_n} + \dfrac{\Delta t}{2T_{SMh}}(U - \Delta P_{gh_n} - \Delta P_{mh_n})\right] \\
F_{31}(x_n+1,x_n) = (\Delta\omega_{n+1} - \Delta\omega_n) - \dfrac{\Delta t}{2M_{eq}}\times \\
\qquad\qquad \left[(\Delta P_{mth_{n+1}} + \Delta P_{mh_{n+1}} - \alpha\Delta P_{tie_{n+1}} - \Delta P_L - D_{eq}\Delta\omega_{n+1})\right. \\
\qquad\qquad \left. -(\Delta P_{mth_n} + \Delta P_{mh_n} - \alpha\Delta P_{tie_n} - \Delta P_L - D_{eq}\Delta\omega_n)\right] \\
F_{32}(x_n+1,x_n) = (U_{I_{n+1}} - U_{In}) - \dfrac{\Delta t}{2}\times \\
\qquad\qquad \left[K_I\alpha(\Delta P_{tie_{n+1}} - \Delta P_{tie_n}) - \beta_f(\Delta\omega_{n+1} - \Delta\omega_n)\right] \\
F_4(x_n+1,x_n) = (\Delta P_{tie_{n+1}} - \Delta P_{tie_n}) - \dfrac{\Delta t}{2}\times \\
\qquad\qquad \left[T_{12}(\Delta\omega_{1_{n+1}} - \Delta\omega_{1_n}) - (\Delta\omega_{2_{n+1}} - \Delta\omega_{2_n})\right]
\end{cases}
\tag{14.20}
$$

In our problem of LFC, the Newton-Raphson iterates are:

$$(J)^k[\Delta x_{n+1}]^k = -[F]^k \tag{14.21}$$

$$\begin{pmatrix} J_1 & J_2 & J_3 & J_4 & J_5 & J_6 \\ J_7 & J_8 & J_9 & J_{10} & J_{11} & J_{12} \\ J_{13} & J_{14} & J_{15} & J_{16} & J_{17} & J_{18} \\ J_{19} & J_{20} & J_{21} & J_{22} & J_{23} & J_{24} \\ J_{25} & J_{26} & J_{27} & J_{28} & J_{29} & J_{30} \\ J_{31} & J_{32} & J_{33} & J_{34} & J_{35} & J_{36} \end{pmatrix}^k \begin{pmatrix} \Delta X_1(1) \\ \Delta X_2(1) \\ \Delta X_3(1) \\ \Delta X_4 \\ \Delta X_1(2) \\ \Delta X_3(2) \end{pmatrix}^k = \begin{pmatrix} F_1(1) \\ F_2(1) \\ F_3(1) \\ F_4 \\ F_1(2) \\ F_3(2) \end{pmatrix}^k \tag{14.22}$$

The state vector is given by:

$$[X] = [\Delta P_{g_1} \quad CV_1 \quad \Delta P_{HP_1} \quad \Delta P_{LP_1} \quad \Delta P_{gh_1} \quad \Delta P_{mh_1} \quad \Delta\omega_1 \quad U_{I_1} \quad \Delta P_{tie}$$
$$\Delta P_{g_2} \quad CV_2 \quad \Delta P_{HP_2} \quad \Delta P_{LP_2} \quad \Delta\omega_2 \quad U_{I_2}]^t \tag{14.23}$$

The Jacobian matrix J is given by:

$$J = \begin{bmatrix} \frac{dF_1(1)}{dX_1(1)} & \frac{dF_1(1)}{dX_2(1)} & \frac{dF_1(1)}{dX_3(1)} & \frac{dF_1(1)}{dX_4} & \frac{dF_1(1)}{dX_1(2)} & \frac{dF_1(1)}{dX_3(2)} \\ \frac{dF_2(1)}{dX_1(1)} & \frac{dF_2(1)}{dX_2(1)} & \frac{dF_2(1)}{dX_3(1)} & \frac{dF_2(1)}{dX_4} & \frac{dF_2(1)}{dX_1(2)} & \frac{dF_2(1)}{dX_3(2)} \\ \frac{dF_3(1)}{dX_1(1)} & \frac{dF_3(1)}{dX_2(1)} & \frac{dF_3(1)}{dX_3(1)} & \frac{dF_3(1)}{dX_4} & \frac{dF_3(1)}{dX_1(2)} & \frac{dF_3(1)}{dX_3(2)} \\ \frac{dF_4}{dX_1(1)} & \frac{dF_4}{dX_2(1)} & \frac{dF_4}{dX_3(1)} & \frac{dF_4}{dX_4} & \frac{dF_4}{dX_1(2)} & \frac{dF_4}{dX_3(2)} \\ \frac{dF_1(2)}{dX_1(1)} & \frac{dF_1(2)}{dX_2(1)} & \frac{dF_1(2)}{dX_3(1)} & \frac{dF_1(2)}{dX_4} & \frac{dF_1(2)}{dX_1(2)} & \frac{dF_1(2)}{dX_3(2)} \\ \frac{dF_2(2)}{dX_1(1)} & \frac{dF_2(2)}{dX_2(1)} & \frac{dF_2(2)}{dX_3(1)} & \frac{dF_2(2)}{dX_4} & \frac{dF_2(2)}{dX_1(2)} & \frac{dF_2(2)}{dX_3(2)} \end{bmatrix} \tag{14.24}$$

The new solution at the iteration $k+1$ is calculated using the flowing equation:

$$x^{k+1} = \Delta x^k + x^k \tag{14.25}$$

1. The initial condition values x^0 are fixed.
2. The convergence of iterative Newton-Raphson is based on the max absolute error $\max |F(x^{k+1})|$ and the specified tolerance $\epsilon = 10^{-6}$.
3. If $\max|F(x^{k+1})| < \epsilon$, iterative Newton-Raphson have converged.

With: $i = 1 : ng$ number of area, and $j = 1 : m$ number of machines; (In our case $ng = 2$ and $m = 30$).

14.4 Fuzzy Logic Control

Nowadays, one of promising control methods in industrial automation and process control is the Fuzzy Logic Control (FLC). Because of simplicity, robustness, and reliability fuzzy logic is used in almost all research areas, including solving a wide range of control problems in power system control and operation. Fuzzy logic is an intelligent technique developed by Professor Lotfi Zadeh. He first introduced the theory of fuzzy sets and fuzzy logic in 1965 when he wrote his first paper entitled Fuzzy Sets (Pothiya and Ngamroo 2008; Shayeghi et al. 2008). This logic is the mathematical representation of the formation of human concepts and of reasoning concerning human concepts. Several published papers have shown and proven that fuzzy systems are strong and efficacy solution schemes. Moreover, the FLC is used in many commercial, domestic, automotive control applications, and has been successfully applied to many control problems (e.g. washing machines, televisions and photocopiers) because no mathematical modeling is involved. This work addresses the problem of tuning the optimal PID controller parameters using fuzzy logic strategy. Our aim in this work is to design a robust load frequency controller based Fuzzy Logic-PID controller to regulate the system frequency concerning large wind power penetration. A general scheme for Fuzzy Logic-PID controller based LFC system is designed as depicted in Fig. 14.9. As shown, the parallel combination between Fuzzy Logic and PID controller is adopted in this system. The Fuzzy Logic controller is implemented in three phases given as follow:

1. Fuzzification module (Fuzzifer).
2. Rule base and Inference engine.
3. Defuzzification module (Defuzzifier).

For the purpose of load frequency control analysis, the inputs of the fuzzy logic controller are the variables error (ACE) and change of error ($dACE$), and the outputs of the fuzzy logic are the PID parameters. The K_P, K_I, K_D values are calculated out according to offline rules in fuzzy controller.

A label set corresponding to linguistic variables of the input control signals, $ACE(Z)$ and $dACE(Z)$, with a sampling time of 0.01 s is as follows:

$$Li(ACE, dACE) = (NB, NS, ZE, PS, PB) \tag{14.26}$$

A label set corresponding to linguistic variables of the output control signals is as follows:

$$Lo(K_P, K_I, K_D) = (ZE, PS, PM, PB) \tag{14.27}$$

The membership function for the control input variables are shown in Fig. 14.10, and the membership function for the control output variables are given as shown in Fig. 14.11.

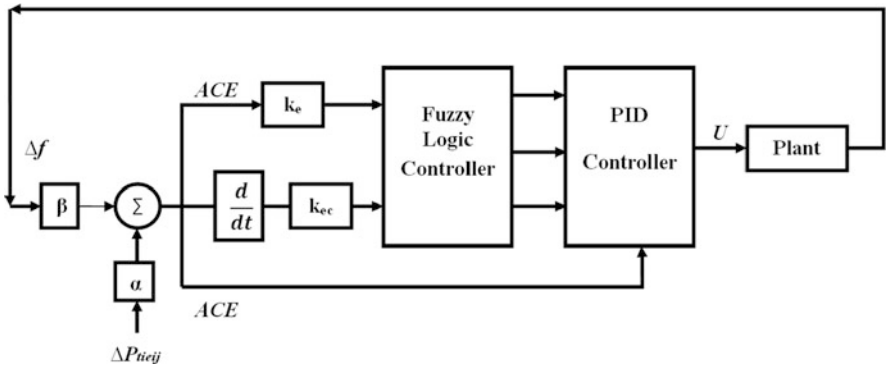

Fig. 14.9 Structure of fuzzy logic-PID controller

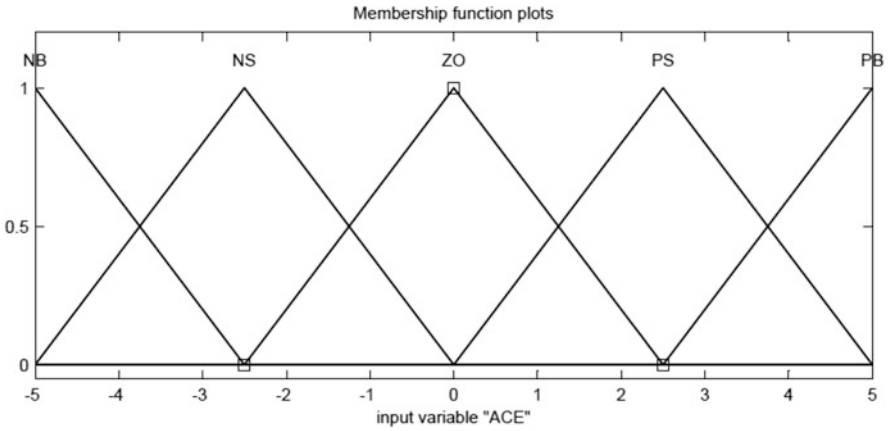

Fig. 14.10 Membership function for the control input variables

The control rules are built from the statement: if input a and input b then output Z, while Table 14.1 resumes the control rules used in this work. In this work the Triangular membership functions is used. The two input signals $(ACE, dACE)$ are converted to fuzzy numbers first in fuzzifier using five membership functions (NB, NS, ZE, PS, PB). Then they are used in the rule table shown in Table 14.1 to determine the fuzzy number of the compensated output signals. The proposed FLC model is shown in Fig. 14.12. The Fuzzy Logic Controller(FLC) is used to reach the optimal PID controller parameters. The proposed approach is compared to the heuristic Particle Swarm Optimization (PSO) technique, and to the classical Ziegler-Nichols method.

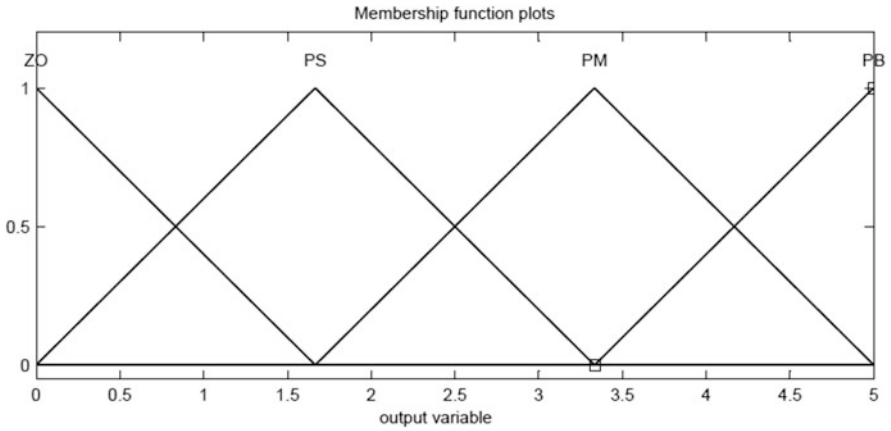

Fig. 14.11 Membership function for the control output variables

Table 14.1 Control rules

	ACE				
$dACE$	NB	NS	ZE	PS	PB
NB	PB	PB	PB	PB	PS
NS	PB	PM	PM	PB	PB
ZE	PB	PM	ZE	PB	PB
PS	PB	PM	PM	PM	PB
PB	PS	PB	PM	PM	PB

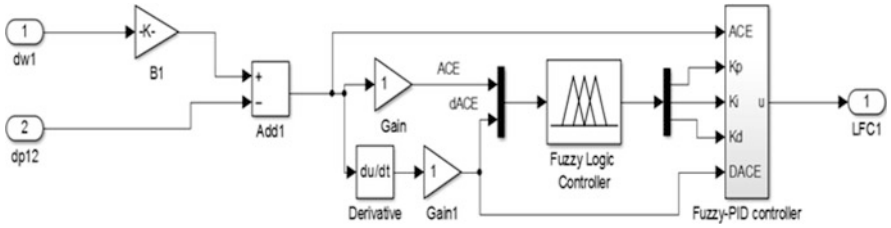

Fig. 14.12 Proposed fuzzy logic-PID controller structure

14.5 Wind Power Generation System

The increasing share of fluctuating renewable energy sources (RES) in the electrical networks poses new challenges for power systems operation and control. On the one hand, renewable energy sources can cover part of the increasing demand and provide electricity production with low marginal costs and reduce CO_2 emissions. In the other hand, large RES integration could influence the power quality and disturb the system stability. Presently, the grid integration of variable distributed generations (DG), such as wind power plants presents one of the most important issues in power system stability and control. Among all renewable energy sources,

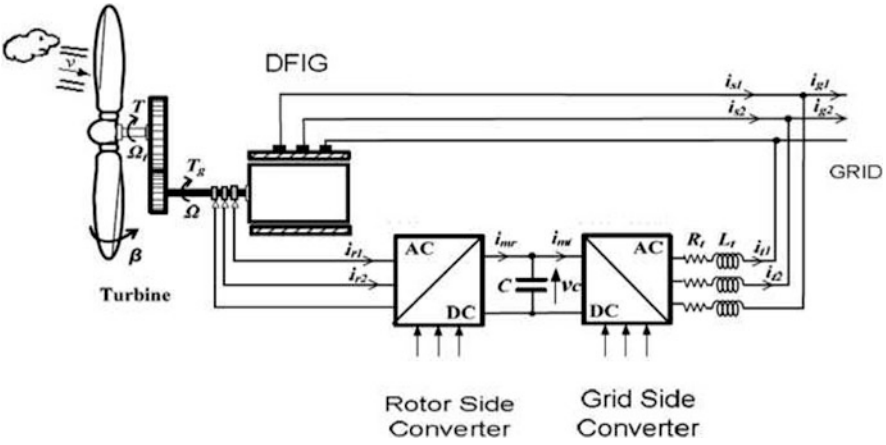

Fig. 14.13 Doubly fed induction generator model

the wind power is the most used in power system. Wind energy is a renewable electricity production from converting kinetic energy of moving air masses into electricity. The wind power is the most renewable energy source utilized in power systems, while this energy depends on the fluctuating nature of the wind direction and its velocity. In the last decades, wind turbines are effectively displacing classical generators and their rotating machinery (e.g. thermal, gas, or nuclear). Nowadays wind power plays an important role in the generation of electrical power as a single wind power plant with operational capabilities similar to a conventional power plant (Jafarian and Ranjbar 2013; Mandal et al. 2014; Wang and McCalley 2013). Therefore, the large deployment of wind turbine led to significant generation shares of wind farms in electrical power networks. Currently, wind power technology is becoming very important, while in the wind farms construction, the variable-speed wind turbine type is the most used technology. Today the doubly fed induction generator (DFIG) shown in Fig. 14.13 is the most used wind turbine, because of his high power control capability since a partial-scale power converter and variable speed operation. The impact analysis of wind farms on power system stability and control requires the development of suitable models. Many dynamic models of wind farms have been developed by researchers and network operators with different detail levels depending on the scope of the study (Ge et al. 2013; Michigami and Oishi 2001). However, high wind turbines penetration causes many implications in frequency dynamics and making frequency stability and control more challenging. When a large penetration of wind power generation is integrated in a small control area, it influences the area frequency control and the tie-line power flow. For that, it is necessary to study the impact of large-scale integration of wind power into interconnected power systems. Hence, maintaining the frequency stability in the electrical network depending to the active power balance is a necessary requirement for a good power quality. This makes the importance of impact study of wind power

integration into the grid a major issue especially during a contingency, which in the scope of this work. The purpose of this work is to analyze the impact of large wind farm integration in interconnected power system using the wind turbine model. Two hundred wind turbines (of 1.5 MW each) are used to represent a 300 MW wind farm, while the mathematical model of such wind turbine is given below.

14.5.1 Wind Turbine Model

Wind turbines produce electricity by using the power of the wind to drive an electrical generator. The power in the airflow is given by Hang et al. (2016), Schlechtingen et al. (2013), Zhang et al. (2013), Sarrias-Mena et al. (2015), and Attya and Hartkopf (2012):

$$P_{air} = \frac{1}{2}(\rho.S.V^3) \tag{14.28}$$

The extracted power from the wind can be expressed as follows:

$$P_{mech} = \frac{1}{2}(\rho.\pi.R^2.V^3.Cp(\lambda, \beta)) \tag{14.29}$$

The tip-speed ratio λ is defined by:

$$\lambda = \frac{\omega_{tr}.R}{V} \tag{14.30}$$

The power coefficient Cp is given by:

$$Cp(\lambda, \beta) = (\frac{1}{2} - 0,167).\beta.\sin(\frac{\pi.(\lambda + 1)}{18,5 - 0,3.\beta}) - 0,00184.(\lambda - 3).\beta \tag{14.31}$$

Figure 14.14 depicts the 1.5 MW wind turbine simulation model in MATLAB.

14.5.2 Wind Farm Model

Increased penetration of wind farm in the interconnected network poses new challenges to conventional power system operation and control. The impacts of increasing a large wind power penetration on system frequency regulation and active power control are of significant interest in the industry. As a result, there is a rising interest in the supplementary services such as the frequency regulator (i.e. load frequency control) in presence of wind farm. In a traditional interconnected power system (without RES), the purpose of the secondary control LFC is to take

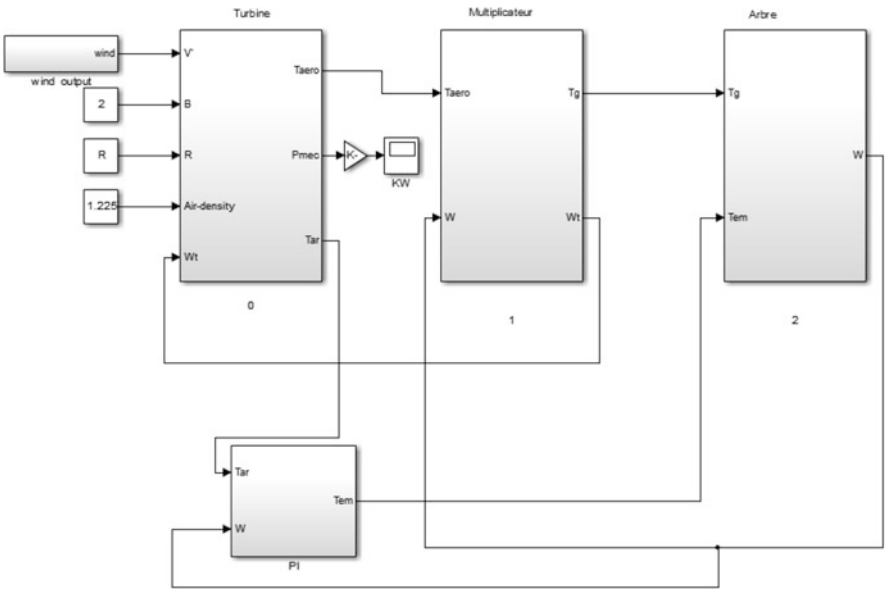

Fig. 14.14 1.5 MW wind turbine simulation model in MATLAB

back the system frequency to nominal value and maintain the balancing between the interconnected control areas. In contrast, due to the fluctuating nature of wind power, equilibrium between production and demand in presence of wind turbines is not an easy operation (Attya and Hartkopf 2012; Vrakopoulou 2013). Wind turbines are non-dispatchable and non-controllable such as the conventional power plants. Therefore, employing the stochastic nature of wind power may result in an adverse effect on the network. Furthermore, the increasing integration of wind farms to satisfy consumption it may has an opposite influence on both frequency control and power quality. It should thus be apparent that it is necessary to design a robust load frequency controller for optimal solution in presence of wind power generation. In a normal state of power system, automatic load frequency control takes place to keep the system within the safety margins, following generation and demand fluctuations. This LFC loop is also depending on the ability of the interconnected network to withstand disturbances. In presence of wind farm, the supply-demand active power mismatch occurs and the frequency will deviate from its nominal value. However, to analyze the additional fluctuation caused by wind farm, optimal LFC controller needs to be employed. The objective is to bring frequency fluctuation back to zero and maintain the power flow on the tie-lines that connect it with the other control areas at its scheduled value. Therefore, each power plant could be controlled using the supplementary frequency control LFC loop (Vrakopoulou 2013). In the case of a high number of wind turbines are installed into a balancing control area, fluctuations in wind power may reduce the balancing areas ability and makes the frequency control more difficult as shown in Fig. 14.15. Towards a stable

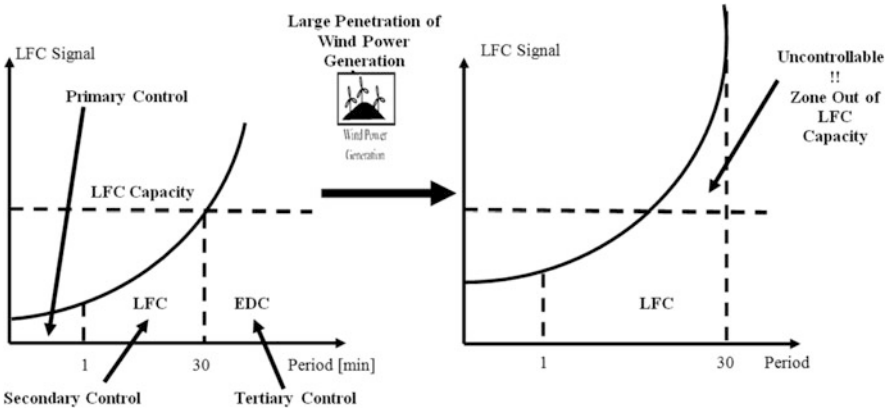

Fig. 14.15 Impact of integration wind farm on LFC

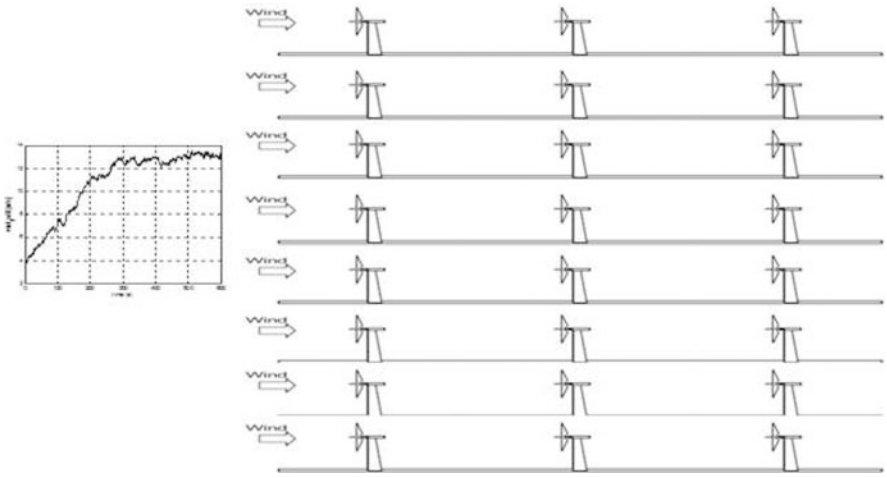

Fig. 14.16 Layout of a typical wind farm

power system operation, the study of possibility of integration a large wind farm in interconnected electrical networks and analysis its impact, an issue which serves as motivation for this work. In this work, a typical wind farm composed of 200 wind turbines of 1.5 MW each is used for the simulation as shown in Fig. 14.16. It is assumed that a large control area is interconnected to a small control area with a large penetration of wind turbines. The wind farm is mapped into eight groups, where each group produces a power of 37.5 MW. This wind farm is based on the wind turbine model, and the wind profile is presented using the dynamic load model proposed by Michigami and Oishi (2001) as shown in Fig. 14.17.

An equivalent wind speed calculated in Eq. (14.32) is applied to the wind farm. We propose that the same wind profile shown in Fig. 14.18 is applied to all wind

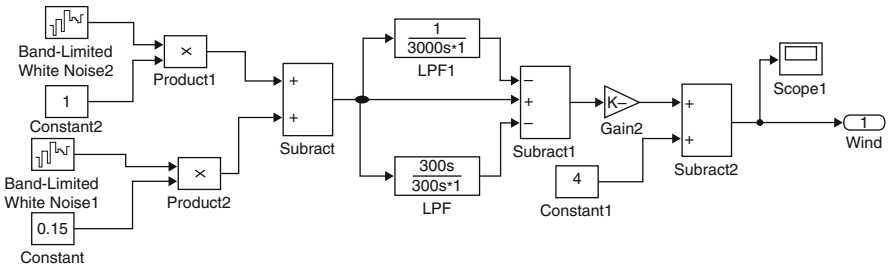

Fig. 14.17 Wind speed model

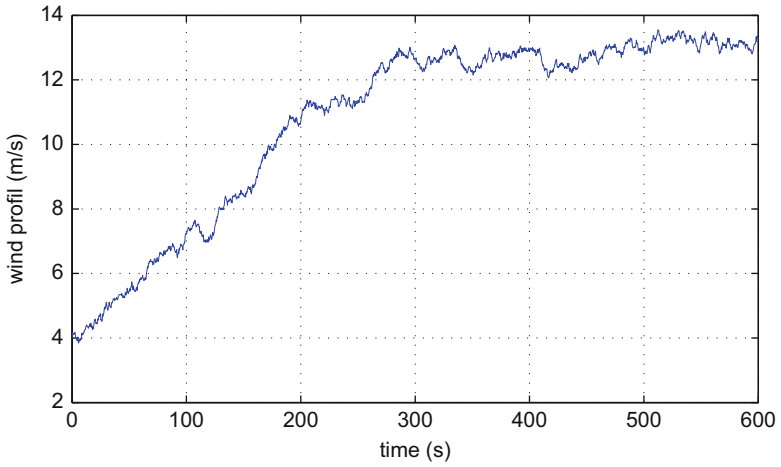

Fig. 14.18 Wind speed output

turbines of the same group: (n_r is number of groups):

$$V_{eq} = \frac{\sum_{i=1}^{i=n} V_i}{n_r} \tag{14.32}$$

The dynamic load model proposed by T. Michigami and T. Ishii is used to represent the wind speed (Michigami and Oishi 2001). The wind speed profile is generated by a block diagram shown in Fig. 14.17. A load consists of base and fringe components obtained from the white noise generators, since the component with period shorter than 5 min or longer than 30 min are out of LFC control, the component is eliminated by applying filters HPF and LPF. The energy penetration of wind farm is defined as:

$$p\ (\%) = \frac{E_w}{E} \times 100\ (\%) \tag{14.33}$$

On the whole and in a simplified manner, the wind farm model is present by:

$$S_{eq} = \sum_{1}^{n} S_i;\ Pm_{eq} = \sum_{1}^{n} Pm_i;\ Q_{eq} = \sum_{1}^{n} Q_i;\ Cp_{eq} = \sum_{1}^{n} Cp_i \tag{14.34}$$

where: the subscript i represents the single turbine.

14.6 Simulation Results and Discussion

To satisfy the load frequency control objectives concerning the integration of wind farm, a dynamic time domain simulation has been carried out using the interconnected IEE Japan East 107-bus, 30-machine. It consists of two areas interconnected by a tie-line power flow. As mentioned, the main goal is to design an effective load frequency controller model with a desirable performance in the presence of large-scale integration of wind turbines. An additional 300 MW wind farm generation is assumed to be installed in area-2. As presented in Sect. 14.5.2, Fig. 14.16 shows the wind farm structure considered in this work. It presents 200×1.5 MW DFIG groups, while the wind farm model operates with the same variable wind profile. All wind turbines are assumed connected to the same PCC. The algorithm developed to analyze the load frequency control LFC is shown in Figs. 14.19 and 14.20. In order to verify the effectiveness of the proposed algorithm, the new LFC model proposed in this work is verified by comparing their responses with those of the conventional LFC based Ziegler-Nichols and the optimal LFC based PSO. The numerical parameters used in the simulation are included in the "Appendix" (Arita et al. 2006) (Tables 14.5, 14.6, 14.7, 14.8, and 14.9).

Using the proposed wind farm model, the impact of wind power fluctuations on the system frequency and tie-line power flow in the two-area interconnected network is examined. Figures 14.21 and 14.22; depict the output power of the first wind turbine and the power coefficient $C_p(\lambda, \beta)$ characteristics respectively. The total wind farm power generation is shown in Fig. 14.23 generation is analyzed. For comparison purpose, four cases are carried out as presented in Table 14.2, whilst the PID controller parameters are given in Table 14.3. The deviations in system frequency and tie-line power flow are shown in Figs. 14.24, 14.25, and 14.26, respectively. It can be seen that the fluctuations of system frequency and tie-line power flow are very important when the penetration of wind power generation is large. However, the system frequency and the tie-line power flow are suppressed most effectively if both areas adopt LFC based optimal PID controller. The effect of the PID controller on the system fluctuations caused by the wind farm is clear that in the difference between the blue corves (without control) and the other corves (using LFC with PID controller). It is clear that in the case of using the conventional LFC design shows more oscillations. In contrast, using the PSO method, global and local solutions could be found simultaneously for a better agreement of the PID controller parameters. Also, these figures show the superior

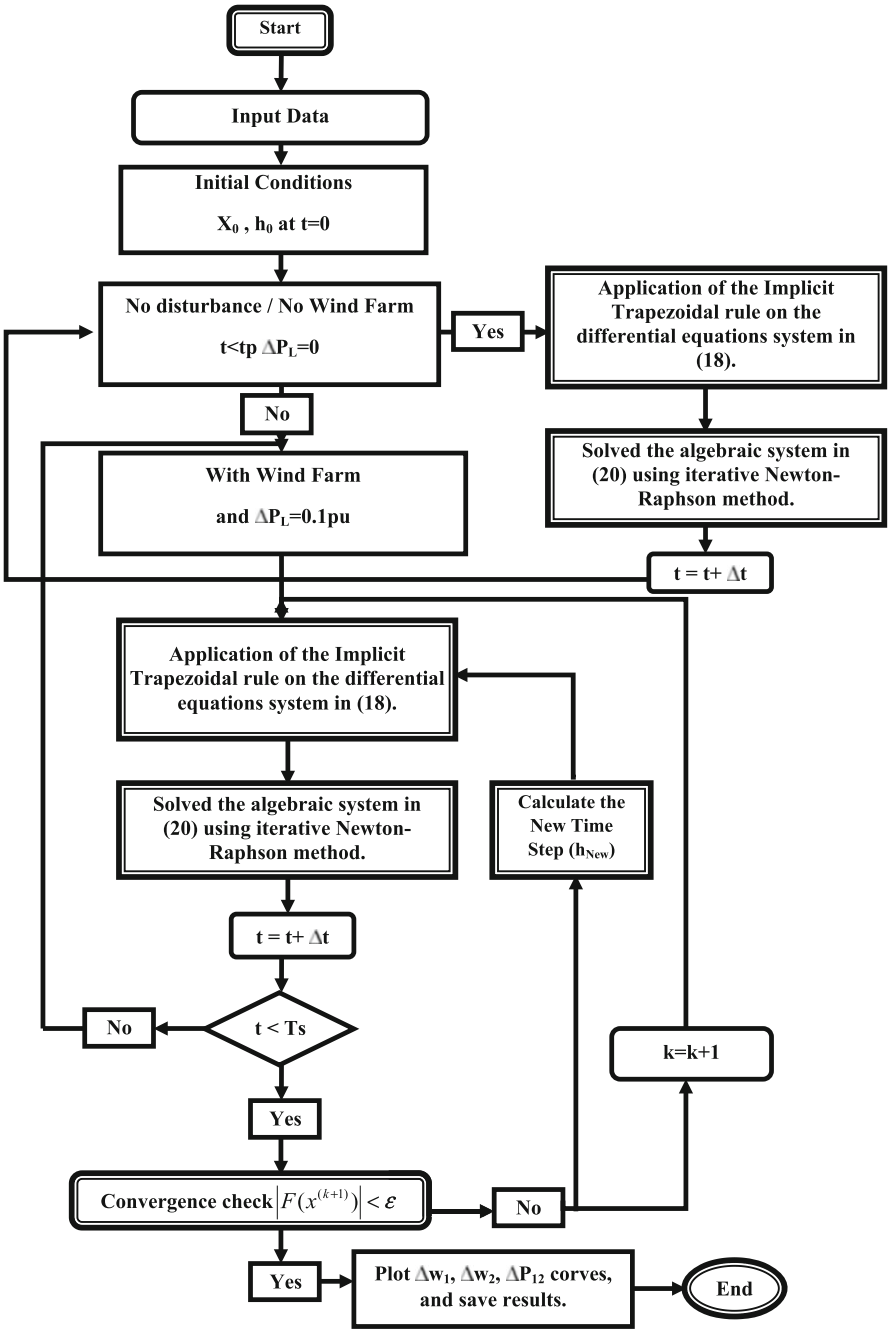

Fig. 14.19 Proposed flowchart for LFC analysis

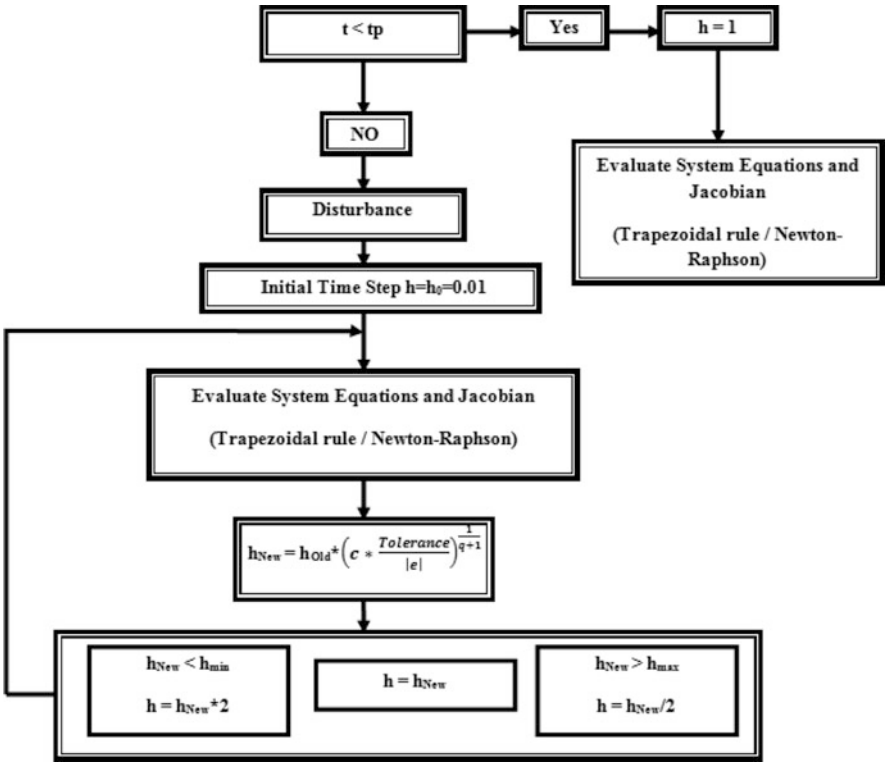

Fig. 14.20 Proposed flowchart for variable time step

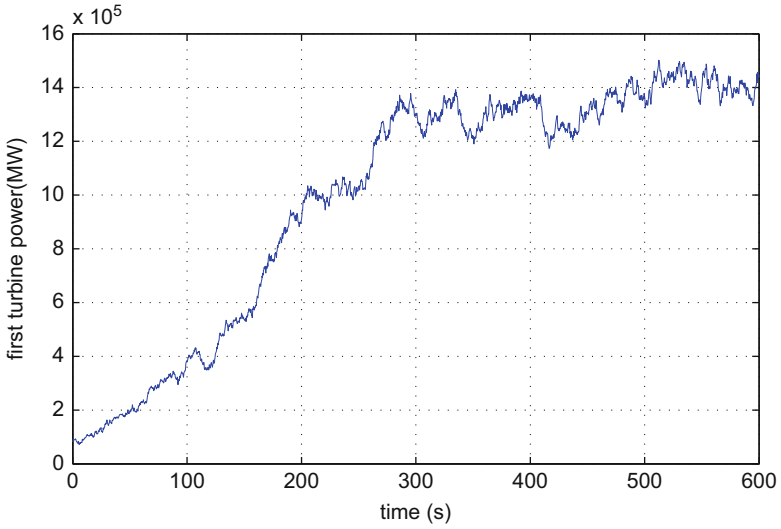

Fig. 14.21 Output power of first wind turbine

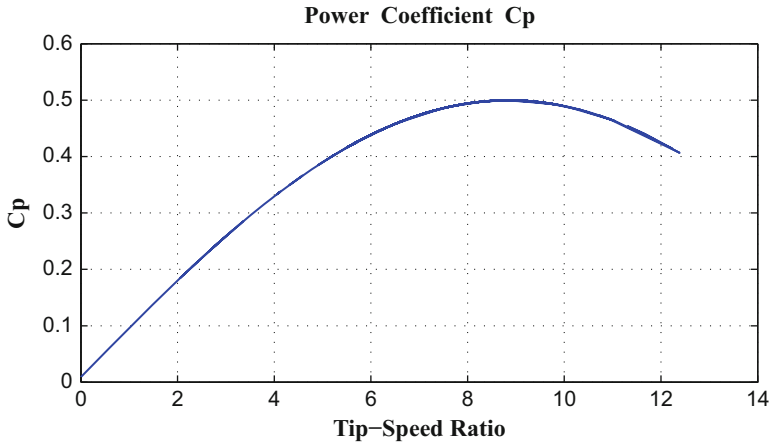

Fig. 14.22 Power coefficient $CP(\lambda, \beta)$ characteristic

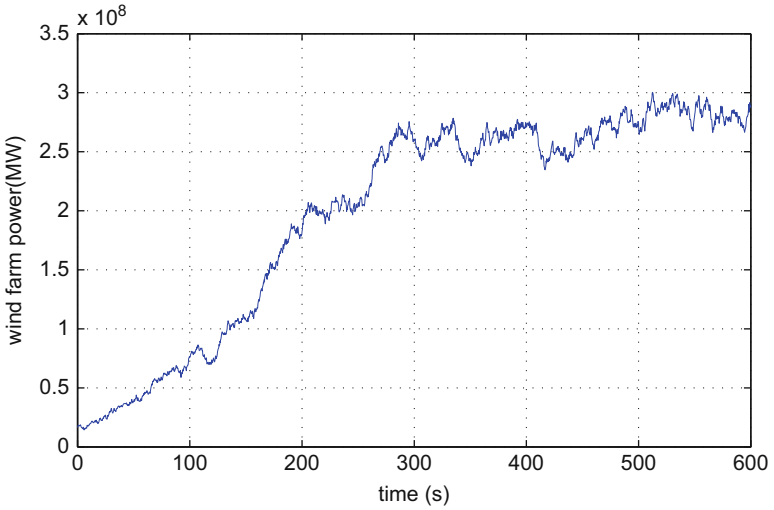

Fig. 14.23 Output power of the wind farm

Table 14.2 Simulation case study

Case 1	Case 2	Case 3	Case 4
Without LFC	Ziegler-Nichols	PSO	Fuzzy-PID

Table 14.3 PID controller parameters

	Parameters		
Methods	K_P	K_I	K_D
Ziegler-Nichols	0.06168	0.0173	0.055
PSO	13.9506	0.2524	1.8796
Fuzzy logic	3.33	1.65	3.33

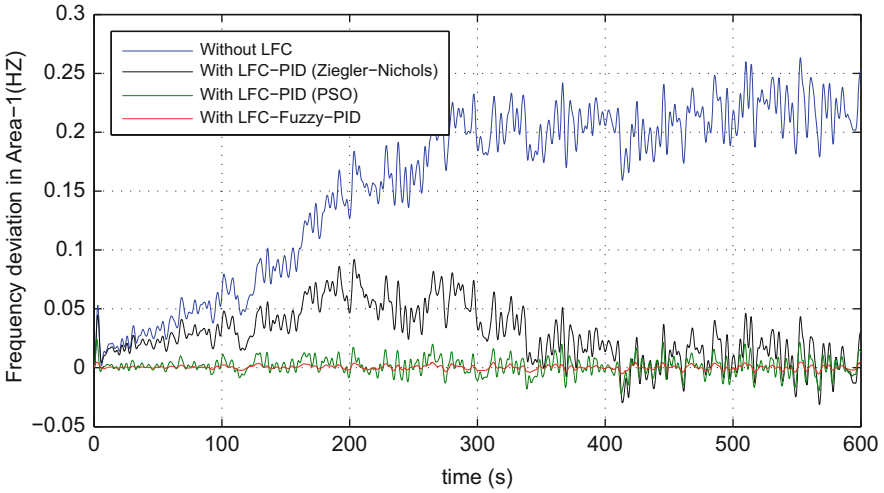

Fig. 14.24 Frequency fluctuation in area-1

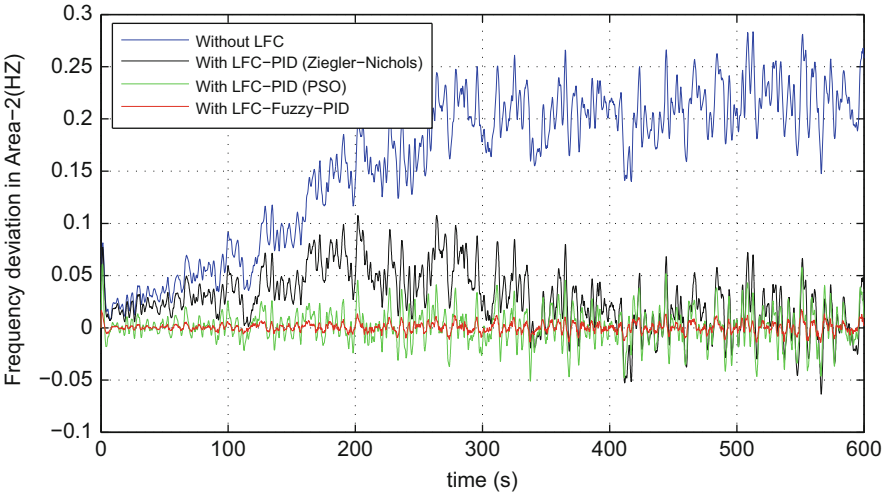

Fig. 14.25 Frequency fluctuation in area-2

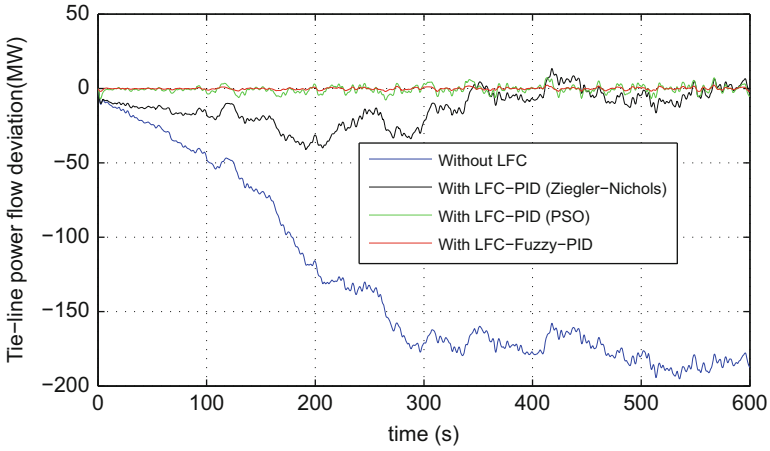

Fig. 14.26 Tie-line power flow fluctuation

Table 14.4 Results and comparison

Tuning PID controller techniques	Without control	Ziegler-Nichols	PSO	Fuzzy logic
Max frequency deviation in Area-1 [Hz]	0.2633	0.09184	0.02176	0.00474
Max frequency deviation in Area-2 [Hz]	0.2827	0.1074	0.05776	0.0148
Max tie-line power flow deviation [MW]	194.1	16.06	3.735	1.044

Table 14.5 Data of the two-area power system

	Area	
Parameters	Area-1	Area-2
Reference frequency [Hz]	50	50
Inertia constant [s]	8.85	9.02
Load-damping constant [pu]	2	2

performance of the proposed Fuzzy Logic-PID controller based LFC scheme to the other conventional and optimal LFC models. Using the proposed Fuzzy Logic-PID controller, the fluctuations of the system frequency and the tie-line power flow are better suppressed compared to the results given by the classical Ziegler-Nichols method and the PSO technique. In other hand, the proposed algorithm based on the implicit integration Trapezoidal rule with variable time step and the iterative Newton-Raphson method is proven to be very efficient for the frequency stability study. The results are compared in view of peak overshoot and settling time; where, the proposed Fuzzy logic-PID controller based LFC scheme is proven to be better as shown in Table 14.4.

Table 14.6 Thermal and nuclear unit parameters

K_G	T_{SR}	T_{SM}	T_{SC}	T_{CO}	F_{HP}	F_{LP}	CV_{close}	CV_{open}	SCV_{min}	SCV_{max}
20	0.2	0.2	0.25	0.9	0.3	0.7	0	1.05	−1000	0.2

Table 14.7 Hydro unit parameters

K_{Gh}	T_{SRh}	T_{SMh}	CV_{close}	CV_{open}	DCV_{min}	DCV_{max}
20	10	0.3	0	1.02	−1000	0.1

Table 14.8 Generation data

Area	Rated capacity [MW]	Initial output [MW]	Inertia constant [Sec]	Total load [MW]
Area-1	53509	30247	8.85	33090
Area-2	11560	10600	9.02	7090

Table 14.9 Wind turbine parameters

Blades number	Rotor diameter	Gearbox ratio	Moment inertia	Coefficient of friction
3	36.5	1 : 104	50	0.0071

14.7 Conclusion

This work investigates the impact of integration a large wind farm on frequency stability and control, which is an important issue in power system control and operation. For this purpose, a Fuzzy Logic structure was proposed to design a new robust load frequency control (LFC) scheme in two-area interconnected power system with diverse sources of power generation concerning high penetration of wind turbines. As the wind power fluctuations influence power system frequency, this study investigated the impact of large wind farm integration on the system frequency and the tie-line power flow in large-scale interconnected electrical network. A typical wind farm equipped with 200 DFIG wind turbines of 1.5 MW each was used for dynamic study, from the frequency stability point of view and control of the electrical power system. The fuzzy logic strategy was used to achieve the optimal values of the PID controller parameters. A new methodology to solve the load frequency control based on the implicit integration Trapezoidal rule with variable time step and iterative Newton-Raphson method was used in this work. The main objective of the proposed algorithm and the suggested LFC scheme is to analyze the frequency stability in an interconnected electrical network in presence of wind farm and solve the frequency fluctuations problem by keeping system frequency and tie-line power interchange between interconnected areas within an acceptable range close to the scheduled values. The proposed strategy was examined on the IEE Japan East 107-bus, 30-machine power system including wind farm, while this system is divided into two control areas: a big control area is interconnected into a small control area. The wind farm is installed in the small control area, where the deviations of the system frequency and the tie-line power

flow in this network are examined to improve the LFC capacity of the conventional power units. The results obtained using the proposed Fuzzy Logic-PID controller based LFC scheme was compared with those of the conventional LFC based Ziegler-Nichols method and the optimal LFC based PSO technique. The results show that the main advantage of using Fuzzy Logic structure is to reduce the fluctuations, while achieving a good performance of the whole response of system in presence of wind farm. Further, the robustness of the proposed control strategy is confirmed and the LFC scheme provides desirable performance against wind power fluctuations.

Appendix

List of Abbreviations and Symbols

Abbreviations

ACE:	Area Control Error.
AGC:	Automatic Generation Control.
ANN:	Artificial Neural Network.
AR:	Area Requirement.
$BFOA$:	Bacterial Foraging Optimization.
$BF-PSO$:	Hybrid Bacterial Foraging and Particle Swarm Optimization.
DEA:	Differential Evolution Algorithm.
$DFIG$:	Doubly Fed Induction Generator.
DG:	Distributed Generations.
EDC:	Economic Dispatching Control.
FA:	Firefly Algorithm.
FLC:	Fuzzy Logic Control.
GA:	Genetic Algorithm.
HPF:	High-Pass Filter.
ISO:	Independent System Operator.
LFC:	Load Frequency Control.
LPF:	Low-Pass Filter.
PCC:	Point of Common Coupling.
PID:	Proportional-Integral-Derivation Controller.
PSO:	Particle Swarm Optimization.
RES:	Renewable Energy Sources.
$TSOs$:	Transmission System Operators.

Symbols

M:	Inertia Constant.
M_{eq}:	Equivalent Inertia Constant.
D:	Load-Damping.
D_{eq}:	Equivalent Load-Damping.
$\Delta\omega$:	Frequency Deviation.
ΔP_m:	Mechanical Power Variation.
ΔP_e:	Electrical Power Variation.
ΔP_L:	Non-Frequency-Sensitive Load Change.
ΔP_{tie}:	Tie-Lien Power Flow Deviation.
ΔP_{mh}:	Hydro Unit Mechanical Power Variation.
ΔP_{mth}:	Thermal Unit Mechanical Power Variation.
ΔP_g:	Thermal Unit Governor Power Variation.
ΔP_{gh}:	Hydro Unit Governor Power Variation.
CV:	Control Valve.
SCV:	Speed Control.
DCV:	Distributor Valve and Gate Servomotor.
CV_{open}, CV_{close}:	Valve or Gate Position Limits.
SCV_{min}, DCV_{min}, SCV_{max}, DCV_{max}:	Valve/ Gate Servomotor Rate Limits.
GF_{min}, GF_{max}:	Speed Governor Limits.
T_{CO}:	Time Constants for the Cross Over.
T_{SC}:	Time Constants for the Steam Chest.
F_{HP}:	High-Pressure Turbine Power Fraction.
F_{LP}:	Low-Pressure Turbine Power Fraction.
K_G:	Thermal Unit Speed Governor Regulation Gain.
K_{Gh}:	Hydro Unit Speed Governor Regulation Gain.
T_{SR}:	Thermal Unit Time Constant of the Speed Relay.
T_{SM}:	Thermal Unit Time Constant of the Servomotor.
T_{SRh}:	Hydro Unit Time Constant of the Speed Relay.
T_{SMh}:	Hydro Unit Time Constant of the Servomotor.
U:	Control Signal.
U_I:	Integral Control Signal.
β_f:	Frequency Bias.
a:	Constant ($a = [1, -1]$).
T_{12}:	Tie-Line Rigidity Factor.
X_{T12}:	Tie-Line Reactance.

T_s:	Simulation Time.
t_p:	Perturbation time.
P_{mech}:	Power from Wind.
ρ:	Air Density.
R:	Blade Radius.
S:	The Swept Area of the Rotor.
V:	Wind Speed.
V_{eq}:	Equivalent Wind Speed.
Cp:	Power Coefficient.
λ:	Tip-Speed Ratio.
β:	Blade Pitch Angle.
w_{tr}:	Turbine Rotation Speed.
E_w:	The Energy Supplied by Wind Farm.
E:	The Energy Supplied by all Generation.
S_{eq}:	Apparent Power of the Whole Wind Farm.
Pm_{eq}:	Equivalent Active Power of the Whole Wind Farm.
Q_{eq}:	Equivalent Reactive Power of Whole Wind Farm.
Cp_{eq}:	Equivalent Power Coefficient of Whole Wind Farm.
$\Delta torh$:	Integration Time Step.
h_{Old}, h_{New}:	Old and New Integration Time Step.
ϵ:	Tolerance.
c:	Constant between the interval [0.6, 0.9].
q:	Order of the Method, for the Trapezoidal Method $q = 2$.
$\|e\|$:	Is a Weighted Root Square Mean Norm.
k:	Iteration Number.

References

Arita, M., Yokoyama, A., & Tada, Y. (2006). Evaluation of battery system for frequency control in interconnected power system with a large penetration of wind power generation. In *IEEE International Conference on Power System Technology*, Chongqing (pp. 1–7).

Attya, A., & Hartkopf, T. (2012). Penetration impact of wind farms equipped with frequency variations ride through algorithm on power system frequency response. *Electrical Power and Energy Systems, 40*, 94–103.

Bevrani, H., & Daneshmand, P. (2012). Fuzzy logic-based load-frequency control concerning high penetration of wind turbines. *IEEE Systems Journal, 6*, 173–180.

Bihui, L., Hong, S., Yong, T., Hongyun, Z., Feng, S., & DongFu, L. (2011). Study on the frequency control method and AGC model of wind power integration based on the full dynamic process simulation program. In *International Conference on Advanced Power System Automation and Protection*, Beijing (pp. 246–251).

Chung, I.-Y., Liu, W., Cartes, D., & Moon, S.-I. (2011). Control parameter optimization for multiple distributed generators in a microgrid using particle swarm optimization. *European Transactions on Electrical Power, 21*, 1200–1216.

Demirören, A., Kent, S., & Günel, T. (2002). A genetic approach to the optimization of automatic generation control parameters for power systems. *European Transactions on Electrical Power, 12*, 275–281.

Eduardo, V.-N., Andreas, S., Oriol, G.-B., Adriã, J.-F., & Marcela, M.-R. (2011). Pitch control system design to improve frequency response capability of fixed-speed wind turbine systems. *European Transactions on Electrical Power, 21*, 1984–2006.

Ge, B., Wang, W., Bi, D., Rogers, C. B., Peng, F. Z., de Almeida, A. T., & Abu-Rub, H. (2013). Energy storage system-based power control for grid-connected wind power farm. *Electrical Power and Energy Systems, 44*, 115–122.

Hang, J., Zhang, J., & Cheng, M. (2016). Application of multi-class fuzzy support vector machine classifier for fault diagnosis of wind turbine. *Fuzzy Sets and Systems, 297*, 128–140.

Hooshmand, R., Ataei, M., & Zargari, A. (2012). A new fuzzy sliding mode controller for load frequency control of large hydropower plant using particle swarm optimization algorithm and kalman estimator. *European Transaction on Electrical Power, 22*, 812–830.

Jafarian, M., & Ranjbar, A. (2013). The impact of wind farms with doubly fed induction generators on power system electromechanical oscillations. *Renewable Energy, 50*, 780–785.

Kassem, A. M., Hasaneen, K. M., & Yousef, A. M. (2013). Dynamic modeling and robust power control of DFIG driven by wind turbine at infinite grid. *Electrical Power and Energy Systems, 44*, 375–382.

Kiaee, M., Cruden, A., Infield, D., & Chladek, P. (2013). Improvement of power system frequency stability using alkaline electrolysis plants. *Proceedings of the Institution of Mechanical Engineers, Part A: Journal of Power and Energy, 227*, 115–123.

Kouba, N. E. Y., Menaa, M., Hasni, M., Boussahoua, B., & Boudour, M. (2014a). Optimal load frequency control based on hybrid bacterial foraging and particle swarm optimization. In *IEEE, 11th International Multi-conference on Systems, Signals and Devices (SSD-PES)*, Barcelona (pp. 1–6).

Kouba, N. E. Y., Menaa, M., Hasni, M., Boussahoua, B., & Boudour, M. (2014b). Optimal load frequency control in interconnected power system using PID controller based on particle swarm optimization. In *IEEE, International Conference on Electrical Sciences and Technology in Maghreb (CISTEM)*, Tunis (pp. 1–8).

Kouba, N. E. Y., Menaa, M., Hasni, M., & Boudour, M. (2014c). Application of artificial neural networks to load frequency control in multi-area power system. In *Proceedings of the 3rd International Conference on Information Processing and Electrical Engineering (ICIPEE)*, Tebessa (pp. 357–362).

Kouba, N. E. Y., Menaa, M., Hasni, M., & Boudour, M. (2016a). Design of intelligent load frequency control strategy using optimal fuzzy-PID controller. *International Journal of Process Systems Engineering, 4*, 41–64.

Kouba, N. E. Y., Menaa, M., Hasni, M., & Boudour, M. (2016b). Frequency stability enhancement in two-area deregulated power system based competitive electricity markets with redox flow batteries and power flow controllers. In *IEEE 8th International Conference on Modelling, Identification and Control (ICMIC)*, Algiers (pp. 1029–1036).

Kouba, N. E. Y., Menaa, M., Hasni, M., & Boudour, M. (2016c). LFC enhancement concerning large wind power integration using new optimised PID controller and RFBS. *IET Generation, Transmission and Distribution, 10*, 4065–4077.

Kouba, N. E. Y., Menaa, M., Hasni, M., & Boudour, M. (2016d). A novel optimal frequency control strategy for an isolated wind-diesel hybrid system with energy storage devices. *SAGE, Wind Engineering, 40*, 497–517.

Liu, P., Yang, W.-T., Yang, C.-E., & Hsu, C.-L. (2015). Sensorless wind energy conversion system maximum power point tracking using Takagi-Sugeno fuzzy cerebellar model articulation control. *Applied Soft Computing, 29*, 450–460.

Mahabuba, A., & Khan, M. (2009). Small signal stability enhancement of a multi-machine power system using robust and adaptive fuzzy neural network-based power system stabilizer. *European Transactions on Electrical Power, 19*, 978–1001.

Mandal, P., Zareipour, H., & Rosehart, W. D. (2014). Forecasting aggregated wind power production of multiple wind farms using hybrid wavelet-PSO-NNS. *International Journal of Energy Research, 28*, 1654–1666.

Michigami, T., & Oishi, T. (2001). Construction of dynamic fluctuation load model and simulation with AFC control of BTB interconnection. *Electrical Engineering in Japan, 136*, 15–25.

Nanda, J., Mishra, S., & Saikia, L. (2009). Maiden application of bacterial foraging-based optimization technique in multiarea automatic generation control. *IEEE Transactions on Power Systems, 24*, 602–609.

Pan, I., & Das, S. (2015). Fractional-order load-frequency control of interconnected power systems using chaotic multi-objective optimization. *Applied Soft Computing, 29*, 328–344.

Panda, S., & Yegireddy, N. (2013). Automatic generation control of multi-area power system using multi-objective non-dominated sorting genetic algorithm-II. *Electrical Power and Energy Systems, 53*, 54–63.

Pandey, S., Mohanty, S., & Kishor, N. (2013). A literature survey on load frequency control for conventional and distribution generation power systems. *Renewable and Sustainable Energy Reviews, 25*, 318–334.

Patnaik, R., & Dash, P. (2015). Impact of wind farms on disturbance detection and classification in distributed generation using modified adaline network and an adaptive Neuro-fuzzy information system. *Applied Soft Computing, 30*, 549–566.

Pothiya, S., & Ngamroo, I. (2008). Optimal fuzzy logic-based PID controller for load-frequency control including superconducting magnetic energy storage units. *Energy Conversion and Management, 49*, 2833–2838.

Prakash, S., & Sinha, S. (2014). Simulation based Neuro-fuzzy hybrid intelligent PI control approach in four-area load frequency control of interconnected power system. *Applied Soft Computing, 23*, 152–164.

Rahmani, M., & Sadati, N. (2013). Two-level optimal load-frequency control for multi-area power systems. *Electrical Power and Energy Systems, 53*, 540–547.

Ramakrishna, K. S. S., & Bhatti, T. S. (2008). Automatic generation control of single area power system with multi-source power generation. *Proceedings of the Institution of Mechanical Engineers, Part A: Journal of Power and Energy, 222*, 1–11.

RamaSudha, K., Vakula, V., & Shanthi, R. V. (2010). PSO based design of robust controller for two area load frequency control with nonlinearities. *International Journal of Engineering Science and Technology, 2*, 1311–1324.

Sahu, R. K., Panda, S., & Padhan, S. (2013). A novel hybrid gravitational search and pattern search algorithm for load frequency control of nonlinear power system. *Applied Soft Computing, 13*, 4718–4730.

Saikia, L., & Sahu, S. (2013). Automatic generation control of a combined cycle gas turbine plant with classical controllers using firefly algorithm. *Electrical Power and Energy Systems, 53*, 27–33.

Saikia, L., Mishra, S., Sinha, N., & Nanda, J. (2011). Automatic generation control of a multi area hydrothermal system using reinforced learning neural network controller. *Electrical Power and Energy Systems, 33*, 1101–1108.

Sarrias-Mena, W., Fernãndez-Ramírez, L., García-Vázquez, C., & Jurado, F. (2015). Dynamic evaluation of two configurations for a hybrid DFIG-based wind turbine integrating battery energy storage system. *Wind Energy, 18*, 1561–1577.

Schlechtingen, M., Santos, I. F., & Achiche, S. (2013). Wind turbine condition monitoring based on scada data using normal behavior models. Part 1: System description. *Applied Soft Computing, 13*, 259–270.

Shayeghi, H., Jalili, A., & Shayanfar, H. (2008). Multi-stage fuzzy load frequency control using PSO. *Energy Conversion and Management, 49*, 2570–2580.

Singh, V., Mohanty, S., Kishor, N., & Ray, P. (2013). Robust H-infinity load frequency control in hybrid distributed generation system. *Electrical Power and Energy Systems, 46*, 294–305.

Tofighi, M., Alizadeh, M., Ganjefar, S., & Alizadeh, M. (2015). Direct adaptive power system stabilizer design using fuzzy wavelet neural network with self-recurrent consequent part. *Applied Soft Computing, 28*, 514–526.

Vrakopoulou, M. (2013). *Optimal decision making for secure and economic operation of power systems under uncertainty*. Ph.D. thesis, Eidgenössische Technische Hochschule ETH, Zürich.

Wang, C., & McCalley, J. (2013). Impact of wind power on control performance standards. *Electrical Power and Energy Systems, 47*, 225–234.

Zhang, W., Wang, J., Wang, J., Zhao, Z., & Tian, M. (2013). Short-term wind speed forecasting based on a hybrid model. *Applied Soft Computing, 13*, 3225–3233.